A V2V Communication System with Enhanced Multiplicity Gain

Qi Zhan, V.K. Varma Gottumukkala, Akihisa Yokoyama, Hlaing Minn
Email: {qi.zhan, hlaing.minn}@utdallas.edu, gvk_v@yahoo.com, ayokoyama@us.toyota-itc.com
University of Texas at Dallas, TX, USA

***Abstract*—Vehicle to vehicle (V2V) communication has gained renewed interest among research community which is further signified by the allocation of dedicated spectrum and an IEEE standard for their usage in recent years. However, 802.11p, the current IEEE standard for vehicular communications, has a relatively low multiplicity (the number of links that it can simultaneously support). In this work, we propose a new vehicular communication scheme based on sectored antennas in order to improve the multiplicity performance. We first show that a sectored antenna based vehicular communication system has higher multiplicity than 802.11p. To further enable multiple transmit sectors to communicate with a receive node simultaneously in a single receive sector, using an OFDMA system design, we propose a new sector-specific pilot design and corresponding channel estimation over time and frequency domains of the channels corresponding to various sectors. Finally, the performance characteristics of the proposed scheme are shown through simulations.**

I. Introduction

Next generation vehicular communications systems possess several characteristics which are substantially different from cellular systems. Such vehicular systems will have multitudes of simultaneous vehicular to vehicular (V2V) communication links. Other characteristics include delay-sensitive safety applications, much higher relative mobility and its effects, different channel and interference characteristics, and different infrastructure with corresponding distinct features. These different requirements and characteristics of vehicular communications impose a communication system design problem which is different from the conventional cellular systems.

Overviews of vehicular communication standards in US and Europe are presented in [1], [2]. The current standard that deals with vehicular communications is IEEE 802.11p [3]. It is based on 802.11a with some parameter scaling for vehicular environments. But there are still several areas where improvement is desired [4], [5]. [6] aimed at enhancing channel utilization of 802.11p. Beam steering techniques to improve connectivity were proposed in [7]. In [8], [9], MAC layer improvements for 802.11p were proposed.

Existing researches on directional antennas focus on MAC or routing protocols. Either no multipath reflections are considered and/or no simultaneous links from one node to many nodes are supported. In [10], vehicles were treated as switch nodes and a dissemination routing method was introduced. [11]–[14] proposed MAC protocols for directional antennas in Ad Hoc wireless networks. There has been some work on sectored antennas in WLAN scenarios [15].

Despite considerable work in literature focused on improving higher layer aspects of 802.11p, there has been limited work on improving physical layer aspects of 802.11p and more so using sectored antennas. The existing research on V2V communications in the physical layer mainly focused on channel measurement and characterization ([5], [16]–[18] and references therein). Multi-antenna systems in V2V channels were considered in [19], [20]. Interference alignment/cancellation was studied in [21]. However, they are all based on omni-directional antennas which limit the capacity for vehicular communications.

In this work, we propose a new approach for mobile V2V communications by introducing highly directional sectored antennas into V2V communications. Our aim is to develop techniques to substantially improve system multiplicity performance. Our contributions include a proposed system with high spatial reuse through highly directional multiple sectored antennas for vehicles, and pilot design and channel estimation scheme tailored to such an environment where multiple simultaneous links are established even within a receive sector.

In the following, we study the improved multiplicity benefits of a sectored antenna based V2V system, the tradeoff relationship between coverage range and the number of simultaneous links and new sector-specific pilot design and channel estimation scheme. Finally, simulation results on the performance characteristics of the proposed system are presented.

II. Coverage and Multiplicity Tradeoff

With the view that future V2V applications will not be constrained within nearby vehicles, we consider all possible/relevant V2V links within the coverage range. Let us now consider the maximum number of vehicles that can be supported by 802.11p in a basic way. Suppose each vehicle needs to transmit 100 bytes of source data in every 100 ms. For 802.11p using QPSK and rate $\frac{1}{2}$ channel code, a vehicle with 100 bytes of source (application)

data will require 17 OFDM symbols plus preamble of length equivalent to 5 OFDM symbols, hence a total of 22 OFDM symbols or 0.176 ms. Each vehicle listens to the "rendezvous" channel during the first 50 ms of each 100 ms frame, and hence the upper limit on the number of successful links that can be supported by 802.11p over 10 MHz channel is 50 ms/0.176 ms = 284. In obtaining these numbers, we assume the cars are scheduled perfectly without any delay or throughput loss in medium access and with no guard intervals between successive communication links. The network efficiency of CSMA used in 802.11a is around 50% [5], and 802.11p will have similar characteristic. As the MAC delay and throughput loss are quite high for 802.11p, the actual number of cars that can be supported by 802.11p is expected to be much smaller than 142 (half of 284). Within the coverage range of 1000 m with 5 lanes and vehicle length of 5 m, there can be over 800 vehicles when the speed is $v = 5$ km/h (traffic jam) and the inter-vehicle distance in time is $t = 0.75$ s, and about 160 vehicles when $v = 64$ km/h (40 m/h) and $t = 1.5$ s. In brief, 802.11p is capable of supporting V2V links of nearby vehicles but may not scale up well for more general application scenarios of V2V links (beyond nearby constraint) within the coverage.

The knowledge of the maximum number of vehicles together with the minimum data rate support for each link will help in system design. For example, suppose each vehicle should communicate with every vehicle within its V2V coverage range of 300 m. There are 69 vehicles within the 300 m coverage range with 5 lanes and inter-vehicle distance of 1 s at 60 km/h vehicle speed. Then, there are roughly $69 * 68/2 = 2346$ paired links (equivalently $69 * 68 = 4692$ unpaired links) for V2V communications within a 300 m coverage range. Clearly such a huge number of links will cause unmanageable interference issues, MAC issues, resource planning issues, etc. The data rate and the number of simultaneous links per frame for a vehicle shape the coverage range and vice versa.

III. Proposed System and Its Advantage

In this work, we propose a new mobile V2V communication system equipped with highly directional sectored antennas (up to 18 sectored antennas). We use a greedy algorithm to estimate the optimum performance of our proposed system. We consider a highway segment of 400 m length with 6 lanes, and each lane has 3.5 m width. At both sides of the highway, we assume there are objects that can reflect wireless signals and the distance between those objects and the nearest lane is half of the lane's width, i.e., 1.75 m. Each vehicle uses 18 directional antennas with the same sector width of 20 degrees unless mentioned otherwise, and each antenna uses the same spectrum and transmit power. Using one of the directional antennas, each vehicle can form a directional link with another vehicle. Directional links operate without interfering with other directional links. Frame length is designed to be relatively small, compared to a vehicle's traveling time from one sector to another. Owing to multiple antennas, multiple simultaneous links can be established with neighboring vehicles. Fig. 1 shows an example of a highway segment with 6 lanes. We assume each car is in the middle of the lane and the distance between two successive cars in the same lane along the horizontal direction is uniformly distributed in the range $[d_{\min}, 2d_{\min}]$ with $d_{\min} = 30$ m. To be more practical, in our simulation we treat the highway segment as circular such that vehicles at one end are immediate neighbors of vehicles at the other end.

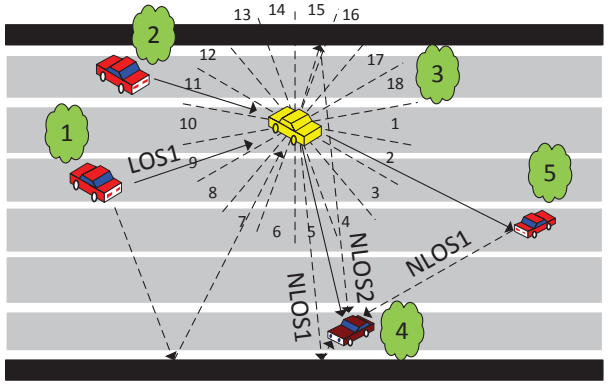

Fig. 1. An illustration of vehicles with 18 sectored antennas

During a symbol interval, a sector can either receive or transmit a signal. In the simulation we assume the antenna radiation outside the intended sector is negligible, and we consider the cars as small rectangle boxes for reflection with 5 m length and 1.8 m width for simplicity. There also exist other propagation mechanisms such as deflection, diffraction, etc, and they can appear as multipath components if coming from the same vehicle or as a signal from another vehicle within the same receive sector. Each receive sector in the proposed system can distinguish signals from different transmit sectors which will be addressed in later sections. In this section we simply consider not more than one successful link at each receive sector, and other signals received at the considered receive sector will be treated as interferences to the desired signal.

The parameters we use in the simulation are as follows. The line-of-sight (LOS) path loss expressions are obtained from [22, Table II, SLDPL, HOTD] and the

non line-of-sight (NLOS) path loss expression from [22, Table III, SLDPL, HOTD]. However, the analysis is still valid for any general path loss model. We consider target SNR as $\mathrm{SNR}_{\mathrm{target}} = 50$dB and noise power spectrum is -204 dBw/Hz. We assume all sectored antennas use the same transmit power, which makes the expected received SNR at 100 m in LOS to be equal to $\mathrm{SNR}_{\mathrm{target}} = 50$dB (effective coverage range is 100 m).

Our goal in this section is to find out how many simultaneous links this system can support when all cars are equipped with 18 sectored antennas and there are both reflections by cars and the walls along the highway. The scheme we use to determine which sector can transmit and which sector should receive is as follows. First, we derive a path loss matrix $\boldsymbol{G}$ (size $18M \times 18M$) between antennas, where M is the number of vehicles on the considered highway segment. We number these vehicles according to their positions along the highway from one end to the other end, and the antennas on each vehicle are numbered clockwise as shown in Fig. 1. So the nth vehicle's mth antenna is numbered as $18(n-1)+m$. There are total of $18M$ antennas in the scenario, and $\boldsymbol{G}(i,j)$ is the path loss between ith antenna and jth antenna. It is calculated by the LOS and NLOS path loss equations.

Each sector antenna can serve as a transmitter as well as a receiver, but one at a time. There are two constraints for the receiver to detect the signal correctly. One is that the SINR at receiver side must be larger than a threshold, the other one is that the desired transmitter should be the only one using the desired transmit sector to communicate with this receiver.

The remaining procedure is as follows. We check every sector antenna one by one and determine whether it can transmit and if so, to which receive sector antenna. Next, if the antenna we check is a receive antenna, it cannot transmit. If not, it can transmit if its interference effects do not cause SINRs of the existing communication links to fall below a target SINR, and if it is the only one using the desired transmit sector to communicate with the receive sector.

Fig. 2 is the illustration of effective communication links when we use 18 sectored antennas on each vehicle. The red dashed line indicates the end of the considered highway segment. As the coverage range is 100 m in our simulation setup and 802.11p uses omni-directional antenna, there are at most 2 communication links that can be supported by an 802.11p channel at the same time. Thus, as shown in Figs. 2, our proposed approach yields a vast improvement of the number of communication links compared to 802.11p.

In Fig. 3, we simulate the above scenario by varying the number of sectored antennas. Simulation settings are the same as above. We simulate 2000 different realizations under each number of sectored antennas. The result shows that the number of simultaneous communication links the system can support generally increases with the number of sectored antennas. An exception is between 8 sectors and 10 sectors where we observe almost the same number of simultaneously supported links. This can be explained as follows. For each car, majority of its communicating partners are in its front or rear areas. When the number of sectors changes from 8 to 10, the number of sectors in front and rear areas and their coverage areas do not change much, thus yielding no noticeable additional links in our evaluation.

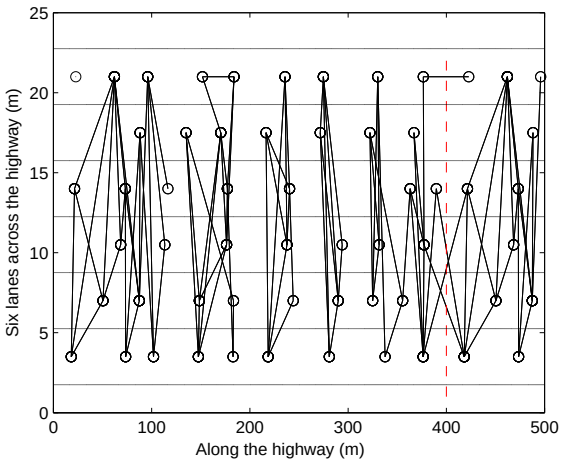

Fig. 2. Simultaneous connection links of vehicles in our proposed approach with 18 sectored antennas (circles = vehicles, lines = connected links).

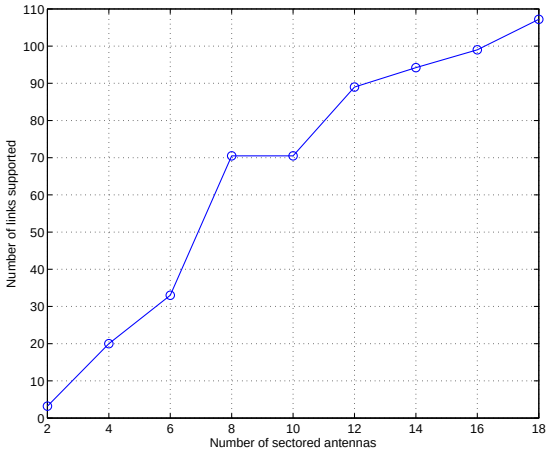

Fig. 3. Number of simultaneous communication links supported by the proposed approach with different numbers of sectored antennas.

In the following sections, in order to effectively enable simultaneous transmission from various transmit sectors to a single receive sector, pilot designs and channel estimation techniques are proposed.

IV. Pilot Designs

To allow several simultaneous links, we adopt OFDMA with 256 subcarriers which are divided into several disjoint subchannels consisting of contiguous subcarriers. To accommodate for different propagation distances, channel delay spreads and timing synchronization errors, we use a cyclic prefix of 6.4 μs (4 times longer than 802.11p) and subcarrier spacing of about 39.1 kHz (1/4 of that of 802.11p). The total bandwidth and the CP overhead ratio remain the same as in 802.11p. Each active link is assigned with a subchannel. In order for a receive sector to distinguish received signals from several simultaneous transmit sectors, the corresponding individual channels need to be estimated reliably. For this, we propose a sector-specific pilot design. For a given receive node, let $\boldsymbol{h}_i$ be the $L \times 1$ discrete-time lowpass-equivalent channel impulse response vector (excluding path loss) between the given receive node and the ith transmit node, where L is the number of channel taps. For the NLOS links, we assume $\boldsymbol{h}_i$ consists of independent, circularly symmetric complex Gaussian entries, i.e. $\boldsymbol{h}_i \sim \mathcal{CN}(\boldsymbol{0}, \boldsymbol{R}_{\boldsymbol{h}_i})$ where $\boldsymbol{R}_{\boldsymbol{h}_i}$ is the channel covariance matrix. For the LOS link, the channel is distributed similar to the NLOS link, with the exception that the first tap has mean $0.5(1+j)$, with j here representing the imaginary unit, and Rician K factor of 1.414. Let $\mathcal{J}$ denote the subcarrier index set of the considered sub-channel, $\boldsymbol{F}_L$ the matrix obtained by taking the first L columns of the standard DFT matrix and $\boldsymbol{F}_{L,\mathcal{J}}$ the matrix obtained by selecting only rows corresponding to $\mathcal{J}$ from $\boldsymbol{F}_L$. Let $\boldsymbol{H}_{\mathcal{J},i} = \boldsymbol{F}_{L,\mathcal{J}}\boldsymbol{h}_i$ denote the channel gain vector for the subcarriers of the desired sub-channel.

In order to select the number of pilot tones, we need to determine the effective number of taps for the channel represented by $\boldsymbol{H}_{\mathcal{J},i}$. We obtain it as the number of significant eigen values of $\boldsymbol{R}_{\boldsymbol{H}_{\mathcal{J},i}} \triangleq \mathrm{E}[\boldsymbol{H}_{\mathcal{J},i}\boldsymbol{H}_{\mathcal{J},i}^H] = \boldsymbol{F}_{L,\mathcal{J}}\boldsymbol{R}_{\boldsymbol{h}_i}\boldsymbol{F}_{L,\mathcal{J}}^H$. For example, with $L = 12$ and sub-channel size of 15 tones, we notice that most of the energy is spread among three eigenvalues and thus three tones would be needed (at the least) to estimate $\boldsymbol{H}_{\mathcal{J},i}$. Minimum mean squared estimation (MMSE) interpolation is used to obtain the channel gains over the remaining tones in the sub-channel and over the remaining symbols in the frame.

Once we fix the number of pilot tones, we design using numerical evaluation the pilot tone locations within the sub-channel. For channel estimation of each transmit sector, three pilot tones are used as described above. Within a sub-channel consisting of 15 tones, we can thus enable estimation of five different transmit sector channels based on one OFDM pilot symbol. The pilots of different transmit sectors within the same OFDM symbol are disjoint. The design criterion for pilot tone locations is minimizing the average of the estimation mean square errors (MSE) of those five channels. Fig. 4 shows the average MSE for different pilot designs for the five pilot sets. The lowest two curves represent the design where all five pilot sets have equally spaced disjoint pilot tones (solid line with square marker) or a slight deviation from that design (dashed line with square marker). The higher curves (solid and dashed lines with non-square markers) correspond to designs substantially different from the above equal-spacing design. We note from the literature that the design with equi-distant pilot spacing is among the optimal ones for several full-bandwidth channel estimators [23]. Although our channel estimator is only for a sub-channel (not full bandwidth), we observe a similar result from Fig. 5. Such a design also offers modularity and simplicity in that pilot locations of different sectors on the same sub-channel are just shifted versions of one another. Thus we propose to use equally spaced pilots within each sub-channel.

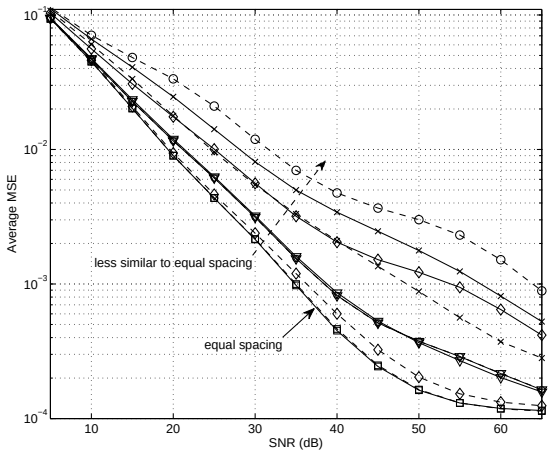

Fig. 4. Performance comparison of different pilot designs (average channel estimation MSE of the five channels corresponding to the links from five different transmit sectors to one receive sector).

If K consecutive pilot symbols are used, the receiving node can estimate channels from $5K$ different transmit sectors to one of its receive sector. In order to track time-varying channels within a frame of several OFDM symbols, we need to insert pilot symbols in several location across the frame. The channel estimation MSE

depends on the number of symbols allotted to pilots as described in the next section.

V. Channel Estimation

The channel estimates on the pilot tones are obtained by dividing the received pilot tones by the corresponding transmit pilot tones. To track the frequency-selective and time-varying channel, the MMSE interpolator is used to obtain the channel gains on the remaining tones and on the data symbols within the frame. Let $\hat{\boldsymbol{P}}_{j,i}$ be the $m_1 \times 1$ channel estimates on the m_1 pilot tones for the ith user in the jth reserved pilot symbol of the frame and $\hat{\boldsymbol{P}}'_i = [\hat{\boldsymbol{P}}^T_{j_1,i}, \hat{\boldsymbol{P}}^T_{j_2,i}, \hat{\boldsymbol{P}}^T_{j_3,i}, \ldots, \hat{\boldsymbol{P}}^T_{j_{m_2},i}]^T$, where m_2 denotes the number of OFDM pilot symbols allocated for each transmit sector within a frame. Let $\hat{H}^{(n)}_{k,i}$ denote the interpolated channel on the kth tone in the nth OFDM symbol within the frame, for the ith user and $\Lambda^{(n)}_{k,i}$ denote the corresponding error in the estimate. Then, using the MMSE interpolation, $\hat{H}^{(n)}_{k,i}$ is given by

$$\hat{H}^{(n)}_{k,i} = \boldsymbol{C}_{H^{(n)}_{k,i}\hat{\boldsymbol{P}}'_i} \boldsymbol{C}^{-1}_{\hat{\boldsymbol{P}}'_i\hat{\boldsymbol{P}}'_i} (\hat{\boldsymbol{P}}'_i - \mu_{\hat{\boldsymbol{P}}'_i}) + \mu_{H^{(n)}_{k,i}} \qquad (1)$$

where $\boldsymbol{C}_{\boldsymbol{xy}} \triangleq \mathrm{E}[(\boldsymbol{x} - \mu_{\boldsymbol{x}})(\boldsymbol{y} - \mu_{\boldsymbol{y}})^H]$ is the covariance matrix between $\boldsymbol{x}$ and $\boldsymbol{y}$, and $\mu_{\boldsymbol{x}} \triangleq E[\boldsymbol{x}]$ is the mean of vector $\boldsymbol{x}$. The channel estimation MSE is then given by

$$\begin{aligned} \mathrm{E}[|\Lambda^{(n)}_{k,i}|^2] &= \boldsymbol{C}_{H^{(n)}_{k,i}H^{(n)}_{k,i}} \\ &- \boldsymbol{C}_{H^{(n)}_{k,i}\hat{\boldsymbol{P}}'_i} \boldsymbol{C}^{-1}_{\hat{\boldsymbol{P}}'_i\hat{\boldsymbol{P}}'_i} \boldsymbol{C}^H_{H^{(n)}_{k,i}\hat{\boldsymbol{P}}'_i}. \end{aligned} \qquad (2)$$

The derivation for the various terms in the above expression is included in the appendix.

VI. Simulation Results and Discussions

A. Simulation Setting

For the current simulation setup, one LOS node and three NLOS nodes communicate simultaneously with the same receive antenna sector of a receive node on the same sub-channel. The receive node is relatively at rest at the origin. The LOS and three NLOS nodes are selected such that their distance is random between 30 m and 50 m. To study the physical layer characteristics, a two slope path loss model is used with the LOS path loss parameters obtained from [22, Table II, SLDPL, HOTD] and NLOS path loss parameters from [22, Table III, SLDPL, HOTD].

OFDMA with $N = 256$ subcarriers and 30 OFDMA symbols per frame is used. Communication within only one sub-channel consisting of 15 tones is considered, where $\mathcal{J}$ denotes the set of tones 1 to 15. The analysis can be extended to other sub-channels too. Three pilot tones are reserved for each transmit sector on a pilot symbol and there are four pilot symbols within a frame for each transmit sector. Transmitter power control is used to compensate for the path loss of each node. For a given SNR, the transmit power for each NLOS and LOS link is adjusted such that the given average SNR is observed at the receiver. The three NLOS links are referred to by NLOS1, NLOS2 and NLOS3. The underlying time-domain channels have $L = 12$ taps and follow exponential power delay profile. For LOS link, the first tap is Rician distributed and the remaining taps are Rayleigh distributed, while for the NLOS links, all taps are Rayleigh distributed. The channel correlation over time follows Jake's model with mobile speed of 120 km/h (to show capability in challenging highly mobile environments). Channels are generated independently after every block of four frames, i.e., 120 symbols. Symbol period is 32 μs (including cyclic prefix) and carrier frequency is $f_c = 5.9$ GHz.

The proposed system uses a sector angle of $20°$, and hence a total of 18 sectors. The antennas pattern gain (in dB) is $A(\theta) = -\min[12(\frac{\theta}{\theta_{3\mathrm{dB}}})^2, A_m]$, where θ ($-180° \leq \theta < 180°$) is defined as the angle between the direction of interest and the boresight of the antenna, $\theta_{3\mathrm{dB}}$ is the 3 dB beamwidth in degrees, and A_m is the maximum attenuation. For our simulation testing, we use $\theta_{3\mathrm{dB}} = 11.67°$ and $A_m = 27.5$ dB.

Data is encoded using half rate convolutional coding with same parameters as 802.11p and interleaved. QPSK modulation is employed on all subcarriers. At the receiver side, soft output maximum likelihood detection is employed followed by deinterleaving and soft Viterbi decoding. Unless otherwise specified, for any given SNR, a 10dB additional power is used for the pilots for better channel estimation.

In all the simulations, we define a parameter Δ which is the SNR difference between the LOS and each of the three NLOS links, i.e. if LOS is at SNR$= x$ dB, the three NLOS are at SNR of $x - \Delta$ dB. In the figures, only the results for NLOS1 among the NLOS nodes are plotted since the other two NLOS nodes, NLOS2 and NLOS3 are at the same SNR as NLOS1 and the results are similar to those seen in the NLOS1 case.

B. Bit Error Rate (BER)

The BER performances for two values of $\Delta = 10$dB and $\Delta = 20$dB are shown in Fig. 5. Increased SNR gives improved BER for both LOS and NLOS nodes. The flat BER curves of NLOS node at low LOS SNR values are simply due to very low SINR values of NLOS node. LOS node achieves a coded BER equal to 10^{-3} at SNR of about 30 dB for $\Delta = 10$dB and at SNR of 18dB for $\Delta = 20$dB. The BERs obtained with perfect channel knowledge are also included to show the effect of imperfect channel estimation. The effect of imperfect

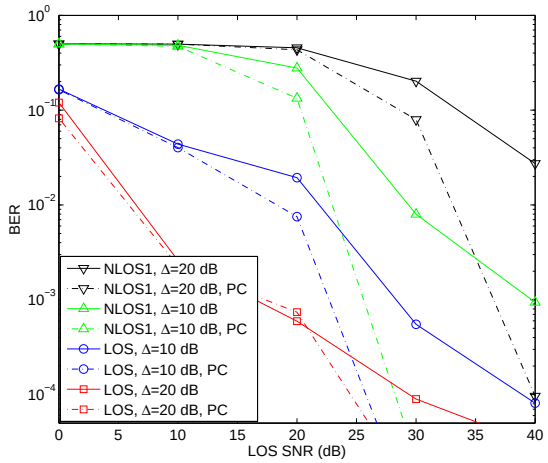

Fig. 5. Coded BER performance with respect to LOS node's SNR for $\Delta = 10$dB and 20dB. PC in the legend indicates perfect channel estimation and interpolation condition.

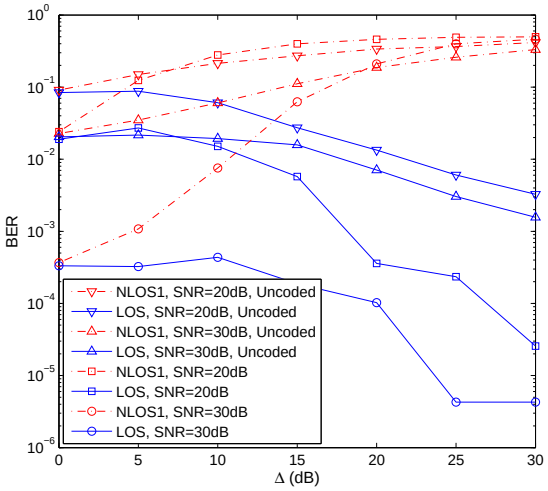

Fig. 6. Effect of Δ on BER (All SNRs in the legend refer to LOS node's SNR. NLOS node's SNR is Δ dB below the LOS node's SNR).

channel estimation/interpolation on BER is significant only at high SNRs. This indicates that the interference due to higher data powers multiplying the lower channel estimation errors at high SNRs is more significant than the interference due to lower data powers multiplying the greater channel estimation errors at lower SNRs.

In Fig. 6, uncoded and coded BERs are plotted over a wide range of Δ values at LOS SNR of 20dB and 30dB. The LOS BER improves while NLOS1 BER degrades with increasing Δ. We also see that coded BER of 10^{-3} or better is achieved for all LOS and NLOS nodes at SNR$=$ 30dB and $\Delta = 0$dB.

C. Further Discussion

The simulations setup above included all 4 nodes transmitting simultaneously on the same sub-channel with the receiver trying to detect all the four links as well. The BER performance could be improved by reducing the number of users allowed to simultaneously transmit on the same sub-channel. We note here that the 802.11p system is designed to allow only one user to transmit at a given time on a specific channel. In addition, although the performance of the proposed approach is presented using a small sector angle of $20°$, which ensures a high multiplicity and spatial reuse, our design can quite flexibly be adapted to other wider sector angle scenarios or higher segmented antennas in front and rear and lower segmented antennas to the side which will enable lower complexity. Next, during initial link establishment, transmitters can use a few subchannels spaced further apart in frequency to capture diversity against fading. But during data transmission phase, a single subchannel can be selected by exploiting channel knowledge. If higher data rate is desired with shorter delay, the proposed system has flexibility of using several subchannels. Finally, the cost of directional antennas is small compared with the value of a car and will decrease substantially after mass production. Thus, due to the great multiplicity gains and good performance obtained with a proper design, the proposed system offers a viable solution to vehicular communications in environments where very high multiplicity is required.

VII. Conclusions

We presented a new vehicular communication system that uses directional (sectored) antennas and OFDMA transmission scheme. We first showed the relatively low multiplicity performance of IEEE 802.11p standard along with the multiplicity benefits possible with a vehicular communications system using directional antennas. Using an OFDMA system model, new sector-specific pilot designs and corresponding estimators for the channels were proposed. The proposed pilot designs enable simultaneous detection of multiple users on the same subchannel at the same time. As evident from the substantial performance improvement of the proposed system by means of large spatial reuse gain via highly directional antennas, together with transmission and receiver processing algorithms for enabling such system, this work offers promising technologies for future vehicular communication systems.

Appendix

For the MMSE interpolator, we have

$$\hat{H}_{k,i}^{(n)} = \boldsymbol{D}_{k,i}^{(n)} \hat{\boldsymbol{P}}_i' + \boldsymbol{Z}_{k,i}^{(n)} \tag{3}$$

$$\mathrm{C}_{\hat{\boldsymbol{P}}'_i\hat{\boldsymbol{P}}'_i} = \begin{bmatrix} \boldsymbol{\alpha}_i+\boldsymbol{\beta}_i & \boldsymbol{\alpha}_i\gamma_i(p_{1,i}-p_{2,i}) & \boldsymbol{\alpha}_i\gamma_i(p_{1,i}-p_{3,i}) & \boldsymbol{\alpha}_i\gamma_i(p_{1,i}-p_{4,i}) \\ \boldsymbol{\alpha}_i\gamma_i(p_{2,i}-p_{1,i}) & \boldsymbol{\alpha}_i+\boldsymbol{\beta}_i & \boldsymbol{\alpha}_i\gamma_i(p_{2,i}-p_{3,i}) & \boldsymbol{\alpha}_i\gamma_i(p_{2,i}-p_{4,i}) \\ \boldsymbol{\alpha}_i\gamma_i(p_{3,i}-p_{1,i}) & \boldsymbol{\alpha}_i\gamma_i(p_{3,i}-p_{2,i}) & \boldsymbol{\alpha}_i+\boldsymbol{\beta}_i & \boldsymbol{\alpha}_i\gamma_i(p_{3,i}-p_{4,i}) \\ \boldsymbol{\alpha}_i\gamma_i(p_{4,i}-p_{1,i}) & \boldsymbol{\alpha}_i\gamma_i(p_{4,i}-p_{2,i}) & \boldsymbol{\alpha}_i\gamma_i(p_{4,i}-p_{3,i}) & \boldsymbol{\alpha}_i+\boldsymbol{\beta}_i \end{bmatrix} - \mu_{\hat{\boldsymbol{P}}'_i}\mu^H_{\hat{\boldsymbol{P}}'_i} \quad (7)$$

where $\boldsymbol{D}^{(n)}_{k,i} \triangleq \mathrm{C}_{H^{(n)}_{k,i}\hat{\boldsymbol{P}}'_i}\mathrm{C}^{-1}_{\hat{\boldsymbol{P}}'_i\hat{\boldsymbol{P}}'_i}$, $\boldsymbol{Z}^{(n)}_{k,i} \triangleq -\boldsymbol{D}^{(n)}_{k,i}\mu_{\hat{\boldsymbol{P}}'_i} + \mu_{H^{(n)}_{k,i}}$. Let $\boldsymbol{f}_k$ be the kth row of $\boldsymbol{F}_L$ and $\mathcal{I}_i$ be the set of pilot tone indices for the ith user. We have

$$\begin{aligned}\mathrm{C}_{H^{(n)}_{k,i}H^{(n)}_{k,i}} &= \mathrm{E}[H^{(n)}_{k,i}H^{(n)H}_{k,i}] - \mu_{H^{(n)}_{k,i}}\mu^H_{H^{(n)}_{k,i}} \\ &= \boldsymbol{f}_k\boldsymbol{R}_{h_i}\boldsymbol{f}^H_k - \boldsymbol{f}_k\mu_{\boldsymbol{h}}\mu^H_{\boldsymbol{h}}\boldsymbol{f}^H_k, \quad (4)\end{aligned}$$

$$\mathrm{C}_{H^{(n)}_{k,i}\hat{\boldsymbol{P}}'_i} = \mathrm{E}[H^{(n)}_{k,i}\hat{\boldsymbol{P}}_i^{'H}] - \mu_{H^{(n)}_{k,i}}\mu^H_{\hat{\boldsymbol{P}}'_i}, \quad (5)$$

$$\mathrm{E}[H^{(n)}_{k,i}\hat{\boldsymbol{P}}_i^{'H}] = [\beta_{1,i},\beta_{2,i},\cdots,\beta_{m_2,i}] \otimes \boldsymbol{f}_k\boldsymbol{R}_{h_i}\boldsymbol{F}^H_{\mathcal{I}_i} \quad (6)$$

where $\beta_{j,i} \triangleq \gamma_i(p_{j,i}-n)$, $\gamma_i(x) \triangleq J_0(2\pi f_{D_i}T_{\mathrm{sym}}(x))$, $p_{1,i},p_{2,i},...,p_{m_2,i}$ are the pilot symbol indices within the frame for the ith user, $J_0(.)$ is the bessel function of zeroth order, $\mu_{\boldsymbol{h}_i} = [0.5(1+j),\boldsymbol{0}_{1\times L-1}]^T$ (j here refers to imaginary unit) for LOS link and $\mu_{\boldsymbol{h}_i} = \boldsymbol{0}_{L\times 1}$ for NLOS1 link, $\mu_{\hat{\boldsymbol{P}}'_i} = \big[(\boldsymbol{F}_{\mathcal{I}_i}\mu_{\boldsymbol{h}_i})^T, \quad (\boldsymbol{F}_{\mathcal{I}_i}\mu_{\boldsymbol{h}_i})^T, (\boldsymbol{F}_{\mathcal{I}_i}\mu_{\boldsymbol{h}_i})^T, \quad (\boldsymbol{F}_{\mathcal{I}_i}\mu_{\boldsymbol{h}_i})^T\big]^T$ and $\otimes$ is the Kronecker product operator. Next, $\mathrm{C}_{\hat{\boldsymbol{P}}'_i\hat{\boldsymbol{P}}'_i}$ is given by equation (7) (shown at the top) where $\boldsymbol{\alpha}_i \triangleq \boldsymbol{F}_{\mathcal{I}_i}\boldsymbol{R}_{h_i}\boldsymbol{F}^H_{\mathcal{I}_i}$, $\boldsymbol{\beta}_i \triangleq \boldsymbol{S}_i^{-1}\boldsymbol{R}_N\boldsymbol{S}_i^{-1}$, $\boldsymbol{S}_i$ is the diagonal matrix with pilot symbols of ith user on its diagonal and $\boldsymbol{R}_N$ is the noise covariance matrix. Using (4),(5), and (7), we can simplify the MSE result in (2).

REFERENCES

[1] J. Kenney, "Dedicated short-range communications (DSRC) standards in the united states," *Proc. IEEE*, vol. 99, no. 7, pp. 1162–1182, July 2011.

[2] E. Strom, "On medium access and physical layer standards for cooperative intelligent transport systems in europe," *Proc. IEEE*, vol. 99, no. 7, pp. 1183–1188, July 2011.

[3] *Wireless LAN Medium Access Control (MAC) and Physical Layer (PHY) Specifications Amendment 6: Wireless Access in Vehicular Environments*, IEEE Standard 802.11p, 2010.

[4] I. Ivan, P. Besnier, M. Crussiere, M. Drissi, L. Le Danvic, M. Huard, and E. Lardjane, "Physical layer performance analysis of v2v communications in high velocity context," in *Proc. ITST*. IEEE, Oct. 2009, pp. 409–414.

[5] L. Cheng, B. Henty, R. Cooper, D. Stancil, and F. Bai, "A measurement study of time-scaled 802.11a waveforms over the mobile-to-mobile vehicular channel at 5.9 GHz," *IEEE Commun. Mag.*, vol. 46, no. 5, pp. 84–91, May 2008.

[6] S. Wang, C. Chou, K. Liu, T. Ho, W. Hung, C. Huang, M. Hsu, H. Chen, and C. Lin, "Improving the channel utilization of IEEE 802.11p/1609 networks," in *Proc. WCNC*. IEEE, Apr. 2009, pp. 1–6.

[7] V. Navda, A. Subramanian, K. Dhanasekaran, A. Timm-Giel, and S. Das, "Mobisteer: using steerable beam directional antenna for vehicular network access," in *Proc. 5th ICMSAS*. ACM, 2007, pp. 192–205.

[8] Y. Wang, A. Ahmed, B. Krishnamachari, and K. Psounis, "IEEE 802.11p performance evaluation and protocol enhancement," in *Proc. ICVES*. IEEE, Sept. 2008, pp. 317–322.

[9] W. Alasmary and W. Zhuang, "Mobility impact in IEEE 802.11p infrastructureless vehicular networks," *Ad Hoc Networks*, pp. 1–5, Sept. 2010.

[10] W. Chen, R. Guha, J. Lee, R. Onishi, and R. Vuyyuru, "A multi-antenna switched links based inter-vehicular network architecture," in *Proc. VNC*. IEEE, Oct. 2009, pp. 1 –7.

[11] C. Chigan, V. Oberoi, J. Li, and Z. Wang, "RPB-MACn: A relative position based collision-free MAC nucleus for vehicular ad hoc networks," in *Proc. IEEE Globecom*, Dec. 2006, pp. 1 –6.

[12] Y. Ko, V. Shankarkumar, and N. Vaidya, "Medium access control protocols using directional antennas in ad hoc networks," in *Proc. INFOCOM 2000.*, vol. 1. IEEE, Mar. 2000, pp. 13–21.

[13] T. Korakis, G. Jakllari, and L. Tassiulas, "CDR-MAC: A protocol for full exploitation of directional antennas in ad hoc wireless networks," *IEEE Trans. Mobile Comput.*, vol. 7, no. 2, pp. 145–155, Feb. 2008.

[14] W. Lai, K. Tseng, and J. Chen, "Mars: a multiple access scheme with sender driven and reception first for smart antenna in ad hoc networks," *Wireless Commun. and Mobile Comput.*, vol. 9, no. 2, pp. 197–208, Feb. 2009.

[15] A. Subramanian, H. Lundgren, and T. Salonidis, "Experimental characterization of sectorized antennas in dense 802.11 wireless mesh networks," in *Proc. tenth ISMAHNC*. ACM, 2009, pp. 259–268.

[16] A. Thiel, O. Klemp, A. Paiera, L. Bernadó, J. Karedal, and A. Kwoczek, "In-situ vehicular antenna integration and design aspects for vehicle-to-vehicle communications," in *Proc. 4th EuCAP*. IEEE, Apr. 2010, pp. 1–5.

[17] C. Mecklenbräuker, A. Molisch, J. Karedal, F. Tufvesson, A. Paier, L. Bernadó, T. Zemen, O. Klemp, and N. Czink, "Vehicular channel characterization and its implications for wireless system design and performance," *Proc. IEEE*, no. 99, pp. 1–24, July 2011.

[18] E. Giordano, R. Frank, G. Pau, and M. Gerla, "Corner: A radio propagation model for vanets in urban scenarios," *Proc. IEEE*, vol. 99, no. 7, pp. 1280–1294, July 2011.

[19] G. Acosta-Marum, B. Walkenhorst, and R. Baxley, "An empirical doubly-selective dual-polarization vehicular MIMO channel model," in *Proc. IEEE VTC 2010-Spring*, May 2010, pp. 1–5.

[20] A. Paier, T. Zemen, J. Karedal, N. Czink, C. Dumard, F. Tufvesson, C. Mecklenbrauker, and A. Molisch, "Spatial diversity and spatial correlation evaluation of measured vehicle-to-vehicle radio channels at 5.2 GHz," in *DSP/SPE Workshop 2009. IEEE 13th*, pp. 326–330.

[21] S. Gollakota, S. Perli, and D. Katabi, "Interference alignment and cancellation," in *SIGCOMM Comput. Commun. Rev.*, vol. 39, no. 4. ACM, Oct. 2009, pp. 159–170.

[22] P. Paschalidis, K. Mahler, A. Kortke, M. Peter, and W. Keusgen, "Pathloss and multipath power decay of the wideband car-to-car channel at 5.7 GHz," in *IEEE VTC Spring*, May 2011, pp. 1–5.

[23] H. Minn and N. Al-Dhahir, "Optimal training signals for MIMO OFDM channel estimation," *IEEE Trans. Wireless Commun.*, vol. 5, no. 5, pp. 1158 – 1168, May 2006.